

REPORT

Touchdown of the Hayabusa Spacecraft at the Muses Sea on Itokawa

Hajime Yano,^{1*} T. Kubota,¹ H. Miyamoto,² T. Okada,¹ D. Scheeres,³ Y. Takagi,⁴ K. Yoshida,⁵ M. Abe,¹ S. Abe,⁶ O. Barnouin-Jha,⁷ A. Fujiwara,¹ S. Hasegawa,¹ T. Hashimoto,¹ M. Ishiguro,⁸ M. Kato,¹ J. Kawaguchi,¹ T. Mukai,⁶ J. Saito,¹ S. Sasaki,⁹ M. Yoshikawa¹

After global observations of asteroid 25143 Itokawa by the Hayabusa spacecraft, we selected the smooth terrain of the Muses Sea for two touchdowns carried out on 19 and 25 November 2005 UTC for the first asteroid sample collection with an impact sampling mechanism. Here, we report initial findings about geological features, surface condition, regolith grain size, compositional variation, and constraints on the physical properties of this site by using both scientific and housekeeping data during the descent sequence of the first touchdown. Close-up images revealed the first touchdown site as a regolith field densely filled with size-sorted, millimeter- to centimeter-sized grains.

The most challenging engineering demonstration, as well as the most important scientific goal of the Hayabusa spacecraft (originally called MUSES-C) is the sampling of surface materials of the Apollo-type, near-Earth asteroid 25143 Itokawa (previously 1998 SF36). To maximize scientific promises of laboratory analyses of the returned samples, it is necessary to characterize physical and geological contexts of sampling sites as much as possible by using both onboard science instruments and housekeeping data of the spacecraft.

The Hayabusa spacecraft arrived at the asteroid hovering at a 20-km altitude (gate position) on 12 September 2005 UTC (1, 2). At altitudes of 7 to ~20 km above Itokawa's surface, Hayabusa spent 6 weeks performing global remote-sensing measurements (3–5) that revealed a clear dichotomy between boulder-rich rough terrains and low-potential smooth terrains of the asteroid. Shape models show that Itokawa is 550 m by 298 m by 224 m in its circumscribed box size (2).

After completion of the scientific observation phase, the Hayabusa team chose two sampling-site candidates on the basis of scien-

tific merits, judged mainly from optical images and light detection and ranging (LIDAR) topography, as well as technical constraints such as guidance-navigation-control (GNC) accuracy and operational safety during the touchdown sequence (Fig. 1A). These sites were (i) the largest smooth terrain area in the Muses Sea, a part of the adjacent “neck” region between the “head” and “body” parts, which is as wide as ~60 m from the head to the body and ~100 m from north to south and (ii) the largest facet of the rough terrain of the body called Little Woomera (2, 3). Both areas are in the local dayside of the equatorial region during the real-time telemetry coverage from ground stations. They also have relatively flat plains with few obstacles as large as the spacecraft itself (6) and show shallow local surface inclinations such that both high solar-power production and broad telecommunication to Earth are available during all touchdown sequences at a solar angle of ~10°.

The operation team performed two touchdown rehearsals on 4 and 12 November and two imaging navigation tests on 9 November. High spatial resolution images of both candidate sites also were acquired from altitudes

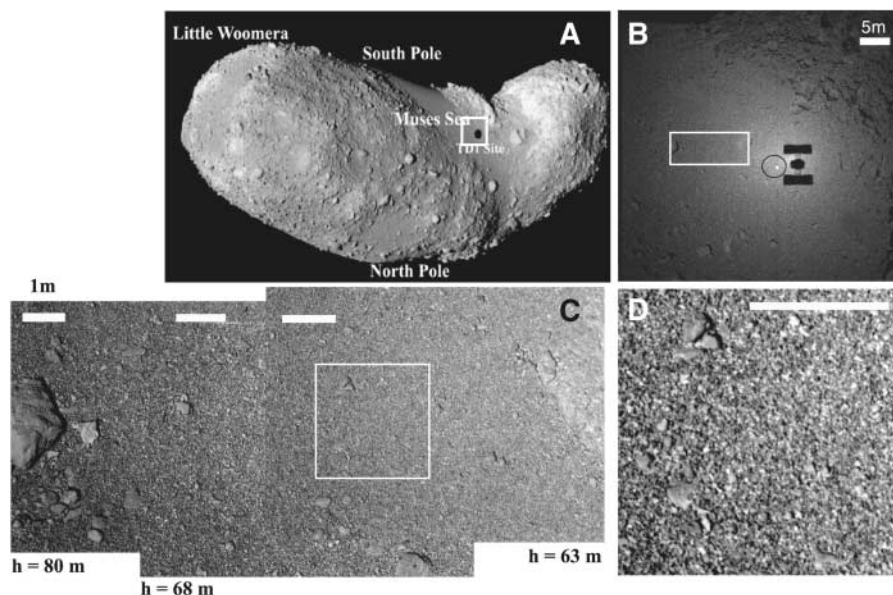


Fig. 1. Location of the Muses Sea smooth terrain, including the first touchdown site on Itokawa. All images were taken in v-band (3). The square in (A) indicates the size of (B); the rectangle in (B) indicates the size of (C); the rectangle in (C) indicates the size of (D). Scale bars in (C) and (D), 1 m. (A) Itokawa is 550 m by 298 m by 224 m in its circumscribed box size (2). (B) Taken by the wide-field optical navigation camera (ONC-W) from ~32-m altitude at 20:33 UTC. The circle next to Hayabusa's shadow shows the target marker that landed on the Muses Sea at TD1. (C) A composite of three close-up images of ST2563511720, ST2563537820, and ST2563607030, which were taken from 80-m, 68-m, and 63-m altitudes, respectively, according to LIDAR measurements. The spatial resolutions are 0.8 to ~0.6 cm/pixel. Contrasts in (C) are arbitrary and stretched to make the apparent brightness of the three images continuous, whereas the gray-scale brightness of (D) is stretched about five times that of the original image. The Muses Sea is composed of numerous, size-sorted granular materials ranging from several centimeters to subcentimeter scales. Rocks larger than tens of centimeters in size often exhibit brighter and/or darker spots on their surfaces than do smaller regolith grains.

¹Department of Planetary Science, Institute of Space and Astronautical Science, Japan Aerospace Exploration Agency, 3-1-1 Yoshinodai, Sagami-hara, Kanagawa 229-8510 Japan.

²Department of Geosystem Engineering, University of Tokyo, Hongo, Tokyo, 113-8656 Japan. ³University of Michigan, Ann Arbor, MI 48109–2140, USA. ⁴Toho Gakuen University, 3-11 Heiwagaoka, Meito, Nagoya, 465-8515 Japan. ⁵Department of Aerospace Engineering, Tohoku University, Sendai, Miyagi, 980-8579 Japan. ⁶Department of Earth and Planetary Science, Kobe University, Kobe, Hyogo, 657-8501 Japan. ⁷Applied Physics Laboratory, Johns Hopkins University, Laurel, MD 20723, USA. ⁸Seoul National University, Seoul, 151-742 Korea. ⁹National Astronomical Observatory of Japan, Mizusawa, Iwate, 023-0861 Japan.

*To whom correspondence should be addressed: E-mail: yano@isas.jaxa.jp

below 7 km, with the telescopic optical navigation camera (ONC-T) equipped with a 1024 by 1024 charge-coupled device of 20 arc sec/pixel resolution and a v-band filter with a central wavelength of 550 nm (3) during each descent [ONC-T is also called Asteroid Multi-band Imaging Camera (AMICA) when it is used for scientific observations (3)]. With these images, the operations team concluded that the Little Woomera area still held too many meter-sized boulders within the GNC accuracy circle of 60-m diameter to conduct a safe descent (7). Thus, the second rehearsal and both of the two actual touchdown attempts on 20 and 26 November 2005 were performed at the Muses Sea area (Fig. 1B).

The smooth terrains cover roughly 20% of the total surface area of Itokawa and mainly concentrate in two areas: the northern polar region and a larger area including the southern polar region and the Muses Sea. These terrains are easily recognized even in low-resolution images because they appear smooth with relatively small brightness contrast. This implies that these terrains are covered with small regolith particles whose grain-size distribution does not vary greatly.

No regional variations were found within spatial resolutions of either the x-ray fluorescence spectrometer (XRS) detecting elements such as Mg, Al, and Si, which were consistent with those of LL or L ordinary chondrites (5), or

the near-infrared spectrometer (NIRS), which was able to measure spectra at 800- to ~2100-nm wavelengths (4) with an ~8-m footprint from a 4.5-km altitude and an ~7-cm footprint during the first touchdown.

Close-up images taken with the ONC-T from altitudes of 80 to 63 m above the touchdown sites provided the highest resolution of ~6 mm/pixel (Fig. 1C). Although grain sizes vary from subcentimeter to ~3 m in this region, it is clear that the Muses Sea is densely filled with size-sorted regolith of similar brightness, mostly ranging from millimeter to centimeter scales, a coarse size that can be classified as “gravel” in the geological term (Fig. 1D). This is far larger than submillimeter regolith powders filling in ponds on 433 Eros (8, 9).

The Muses Sea holds a few boulders larger than several meters across, some of which are surrounded by dips or depressions. The boundary with the body rough terrain has a “transition zone” where boulders appear to exhibit imbrications. Also evident is a gradual decrease of both the average size of regolith particles and the spatial density of large rocks from the transition zone to the center of the Muses Sea. There, these rocks, tens of centimeters in size, often have rounded corners, have flat sides facing down, and tend to collect together. All of the smooth terrains are concentrated in local lows of gravity-centrifugal potential, and the Muses Sea has the minimum

potential over the entire surface of Itokawa (2). These facts suggest a possible comminution and transportation process of regolith materials between the surrounding rough terrains and the Muses Sea smooth terrain, a process that may still be occurring (10, 11).

If the resurfacing process of the Muses Sea is still in progress, both large rocks and sub-surface undulations might have been embedded by regolith that accumulated to similar depth. In this case, the thickness of this region is likely to be more than several meters, which is the typical roughness observed in rough terrains. Nevertheless, possible energy sources for block-regolith interaction/transportation may include electrostatic levitation (mainly for the finest submillimeter components below the best spatial resolution of the ONC-T close-up images) (12), planetary tides during close encounters (13), extreme thermal cycles, impact excavation, and seismic shaking (14).

Hayabusa’s “impact sampler” was designed as a single collection mechanism suitable for a diverse range of target surfaces (15, 16), because surface conditions of Itokawa could not be fully documented from ground observations before the development of the spacecraft. The sampler can operate on targets ranging from metal-silicate hard bedrock to regolith layers with gravel to microparticles. Impact experiments were performed (15) with this sampling system onto various analog materials such as heat-resistant bricks, 200- μ m glass beads, and lunar regolith simulant, at a normal impact incident angle unless otherwise specified both in 1g and in reduced gravity levels ($>10^{-5}g$), by using a 140-m-tall vacuum drop tower at the Micro-Gravity Laboratory (MGLAB) in Gifu, Japan. From the result, the expected amount of the collection mass in the Hayabusa sampler model from 1g and micro-gravity impacts for both bedrocks and regolith were several hundred milligrams to several grams per shot, except oblique impacts at $>45^\circ$, where the collection mass was <100 mg per shot. Additionally, we performed impact tests onto targets consisting of 3- to ~10-mm natural coarse grains and glass balls, which were equivalent in size to the Ta projectiles in the vacuum at 1g. Because of the limit of the experimental setup, we measured only the total ejected mass without using the sampler model. We estimated the collection mass of coarse grain impacts, which were the most likely result of impact sampling at the Muses Sea, to fit values between monolith (i.e., bedrock) and fine regolith (i.e., dust) targets (Fig. 2).

On 19 November UTC (20 November JST), the first touchdown (TD1) resulted in a canceled projectile firing, because the fan beam sensor apparently detected an obstacle, and an avoidance maneuver was conducted. The emergency ascent was autonomously canceled, and the spacecraft continued to free-fall to

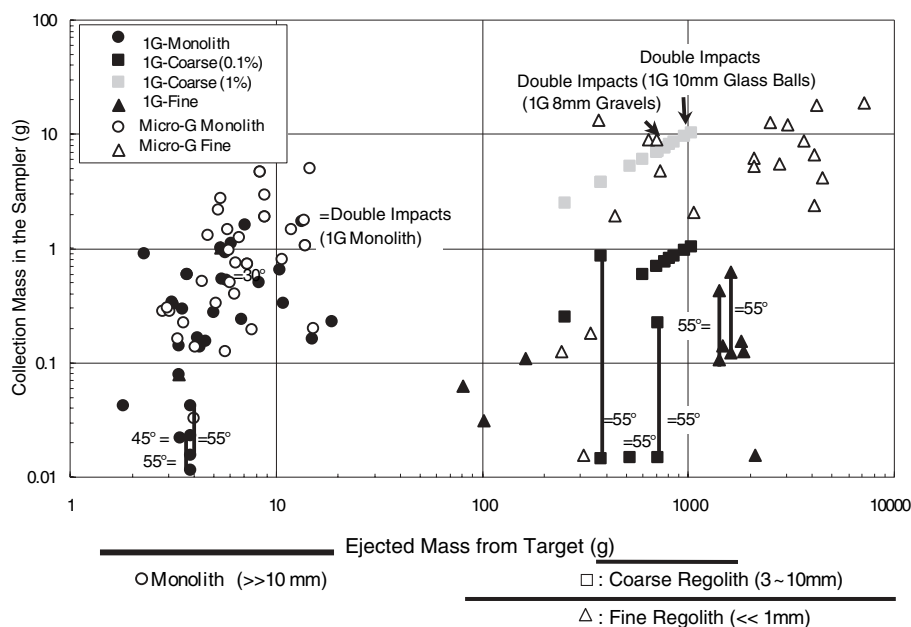


Fig. 2. Collection mass obtained in the Hayabusa impact sampler from impact ejecta mass of bedrocks (monolith) and coarse and fine grains (regolith) in vacuum. Filled shapes are experimental data in 1g, and open shapes are data in microgravity ($10^{-5}g$) using the MGLAB drop tower. Impact angles are normal unless otherwise specified. Inclined impacts at 55° from normal have data ranges between impact ejecta reached to the sampler canister as the maximum and those reached only inside the sampler horn. Shaded legends are coarse-grain impacts in 1g, with 1% collection efficiency assumed. Double impacts indicate the sum of the total sample mass collected by two projectiles that impacted at the same point on the target.

Itokawa's surface. At 21:10 UTC, the sampler horn touched and then rebounded on the asteroid surface near where the target marker landed at 6°S latitude and 39°E longitude in the head side of the Muses Sea. The second bounce occurred at 21:30 UTC. At 21:41 to 22:15 UTC, the spacecraft landed on the southwest of the Muses Sea region, closer to the head part than to the body, until the manual command for an emergency ascent thrust was conducted. Some slow regolith grains (below escape velocity of ~20 cm/s) might have been lifted up by the tip of the horn, and they might have reached the sample canister during the TD1 landing that lasted more than half an hour. Therefore, the hatch of the canister was closed to secure potentially collected samples.

At the second touchdown (TD2) on 25 November UTC (26 November JST), the whole sequence went as planned and the touchdown was detected by measuring deformation of the foldable sampler horn by the laser rangefinder (LRF)-S2 at 22:07 UTC (17). The spacecraft autonomously commanded the firing of two projectiles with a 0.2-s interval and then ascended by using the thrusting reaction control systems. However, after receiving data from the onboard recorder, it was found that the spacecraft might have issued a safeguard command for the projectiles ~4 min before the touchdown (18), which would have overridden the fire

command. At this stage, it remains unclear whether samples were collected during TD2, but the canister was closed to enable its insertion into the return capsule.

Surface characteristics of the Muses Sea area were estimated from altitudes from the center of the spacecraft mass—which were derived by measurements from four beams of LRF-S1 during the TD1 sequence and from stiffness and deformation test results of the prototype and flight model sampler horn in the laboratory (19, 20)—and from bounce time and velocities at the moment of touchdown. In this analysis, we set conditions such that all the LRF-S1 data best approximated to free-fall parabolic curves by least-square fitting in a temporal-altitude plot (Fig. 3A), and the first and second bounces shared a common contact time of 21:09:32 UTC at the asteroid surface. Then, numerical simulation on motion dynamics of the spacecraft was performed to obtain a set of possible surface characteristics satisfying the identified velocity conditions. This simulation was based on the multibody model of the spacecraft, where the sampler horn was modeled as an articulated lumped-mass system connected by compliant hinges (20). By applying Hertz's model and Coulomb's model to the asteroid surface—assumed as a flat, solid plate—the contact force and kinetic friction coefficient were calculated (21–23).

We then estimated the approaching vertical velocity of the spacecraft to the asteroid surface immediately before contact (V_z) as about -6.9×10^{-2} m/s and the bouncing velocity right after the contact (V'_z) as about 5.8×10^{-2} m/s. Thus, the coefficient of restitution of the TD1 site is $\epsilon \sim 0.84$, which is far larger than the value measured for unconsolidated quartz sand targets impacted at 1 to ~100 cm/s (i.e., ~0.01 order) in microgravity (24). Although there was no direct measurement available for the relative horizontal velocity to the surface at the moment of the touchdown (V_x), it is inferred to be greater than 4.5×10^{-2} m/s toward the opposite direction of the attachment position of the sampler horn. Otherwise, the spacecraft cannot have $V'_z \sim 5.8 \times 10^{-2}$ m/s. This is due to asymmetric design of the spacecraft with respect to its center of mass (I). The tumbling motion induced during the surface contact becomes very different depending on such horizontal velocity at the moment of touchdown. If $5.0 \times 10^{-2} > V_x > 4.5 \times 10^{-2}$ m/s for this direction, the value of the friction coefficient of the touchdown surface as the solid plate is estimated as $\mu > 0.8$, or even greater than 1. In such a case, the tip of the sampler horn might have scratched rough but deformable surface materials, or possibly pushed and removed some quantity of them. This view is consistent with the regolith field imaged by

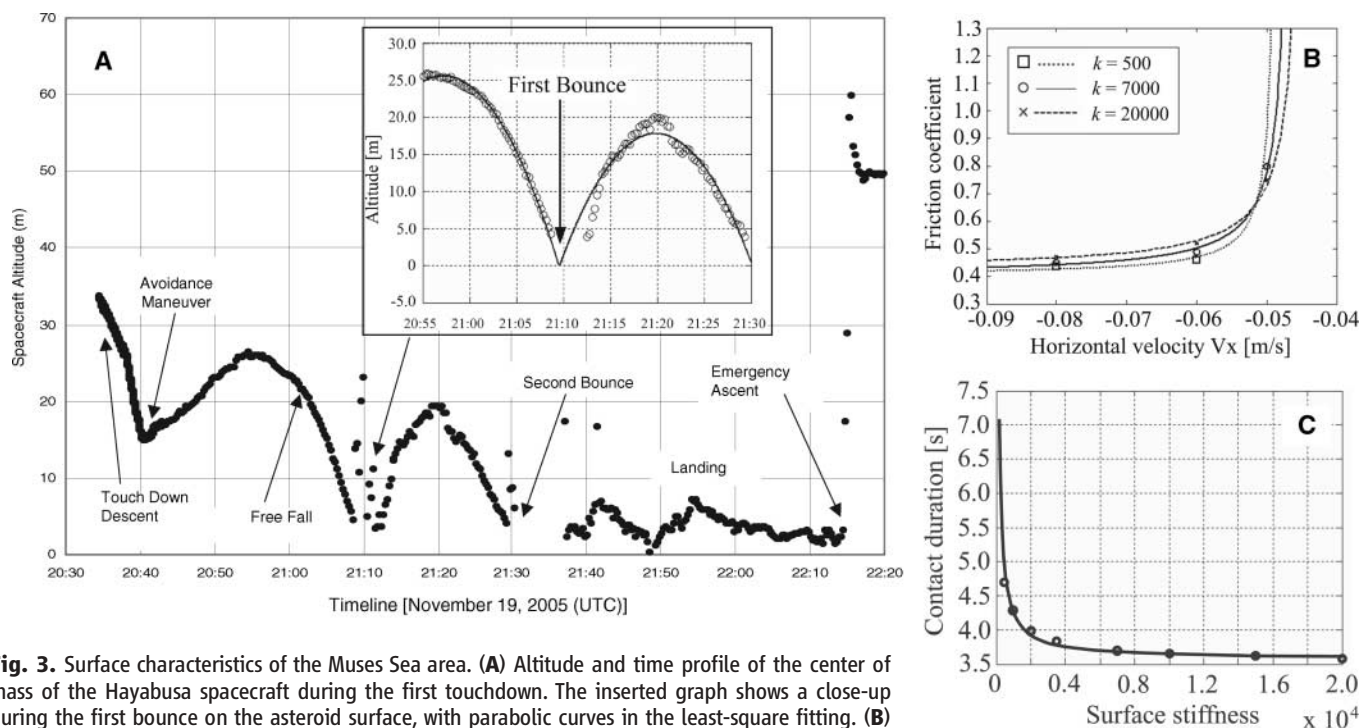


Fig. 3. Surface characteristics of the Muses Sea area. **(A)** Altitude and time profile of the center of mass of the Hayabusa spacecraft during the first touchdown. The inserted graph shows a close-up during the first bounce on the asteroid surface, with parabolic curves in the least-square fitting. **(B)** Simulation results of the friction coefficient (μ) of the asteroid surface, assumed to be a flat, solid plate, and the relative horizontal velocity (m/s), with negative values indicating the opposite direction from the sampler horn with respect to the center of the spacecraft mass at the moment of the first bounce. **(C)** Simulation results of the stiffness ($\text{N/m}^{-1.5}$) of the surface, assumed to be a flat plate, as a function of the contact time(s) during the first bounce in TD1. The surface stiffness is insensitive to the vertical velocity but sensitive to the contact time.

the ONC-T rather than loosely bonded dust layers (25). In this analysis, the result was not as sensitive to the stiffness of the surface as the solid plate (Fig. 3B). It is more sensitive to the time duration of the surface contact, which we do not have in the measured data. The contact duration would have been ~ 3.6 s with $k = 2 \times 10^4$ N/m $^{-1.5}$ and ~ 4.7 s with $k = 5 \times 10^2$ (Fig. 3C).

These first-order estimates still give us the sense that the Muses Sea regolith was not a fluffy, powdery pond in which the tip of the horn would have been embedded but, rather, that the spacecraft would bounce during the touchdown. This insight is important for engineering design constraints of both future sample-return missions and microgravity rovers on asteroids of sizes similar to Itokawa's. It also tells us that a major portion of samples returned to ground laboratories will most likely be coarse-grained regolith and their fragments rather than powdery, submillimeter particles.

A temperature profile from the XRS thermal radiator was also monitored during the TD1 phase (Fig. 4) (26, 27). Its temperature increased by thermal emission from the asteroid surface as the spacecraft descended, but it stopped increasing at 28 ± 2 m altitude above the Muses Sea, when the spacecraft hovered as a result of autonomous obstacle detection and avoidance maneuvers. About 20:53 to $\sim 20:57$ UTC [Fig. 4, part (1)], the radiator temperature almost reached thermal equilibrium, so that the emission temperature

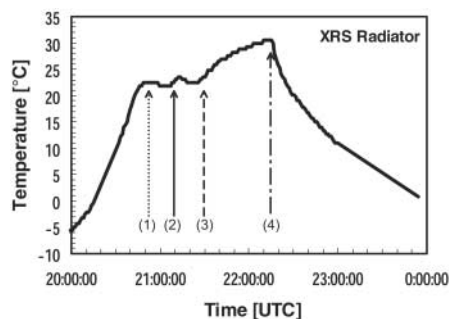


Fig. 4. Direct reading of temperature profile of the XRS radiator during the TD1 sequence before correction with ground calibration data. (1) Its temperature increased until the spacecraft descended to 28 ± 2 m altitude, where an obstacle was detected and the spacecraft conducted avoidance maneuvers. There, the radiator appears to reach a temporal thermal equilibrium. (2) The spacecraft autonomously decided not to escape and finally touched down at the surface at 21:10. (3) After the first bounce, the spacecraft landed on the surface and stayed there for about 40 min, showing a gradual temperature increase. (4) The spacecraft escaped by ground commands with rapid decrease in temperature. The Muses Sea surface temperature is estimated at about 310 ± 10 K, after the calibration with ground test data, in order to equilibrate with the XRS radiator at the period of (1).

from the Muses Sea area below the spacecraft was estimated at 310 ± 10 K, which was equivalent to $+23^\circ\text{C}$ in direct reading (Fig. 4) before the correction with ground calibration data (26, 27). At a solar distance of ~ 1 astronomical unit during the rendezvous with Itokawa, this result favors brecciated rocks and/or a coarse-grain-filled surface with a thermal inertia ($\Gamma = 10^2$ to $\sim 10^3$ Jm $^{-2}$ s $^{-0.5}$ K $^{-1}$) between that of monolithic rocks (e.g., $\Gamma = 4000$ Jm $^{-2}$ s $^{-0.5}$ K $^{-1}$, in which case the surface temperature is expected to be 280 K) and powdery surface like lunar regolith (e.g., $\Gamma = 40$ Jm $^{-2}$ s $^{-0.5}$ K $^{-1}$, the corresponding surface temperature for which is 370 K). This is also supported by the ground-based infrared spectrophotometry of Itokawa [$\Gamma = 750$ Jm $^{-2}$ s $^{-0.5}$ K $^{-1}$ (28)]. This view is consistent with the regolith field images of the Muses Sea. Other possible explanations for the low temperature of the Muses Sea regolith are that the TD1 site might be located at a higher latitude than estimated or that the Muses Sea area had not yet reached the maximum temperature, even at high noon, during TD1 because the area was so concave that duration of daytime was much shorter than in other areas, such as the head and body parts.

Hayabusa represents the first attempt to sample an asteroid surface. If the spacecraft comes back to Earth successfully in June 2010, the samples we have obtained will be surface materials from the Muses Sea. Therefore, understanding their characteristics in structure and composition through both remote sensing measurements and laboratory analyses (29) is vital in bridging current inferences based separately on meteoritic analyses and the ground-observation database of S-type asteroids.

References and Notes

1. J. Kawaguchi *et al.*, *Acta Astronaut.* **52**, 117 (2003).
2. A. Fujiwara *et al.*, *Science* **312**, 1330 (2006).
3. J. Saito *et al.*, *Science* **312**, 1341 (2006).
4. M. Abe *et al.*, *Science* **312**, 1334 (2006).
5. T. Okada *et al.*, *Science* **312**, 1338 (2006).
6. The size of the Hayabusa spacecraft with fully extended solar arrays is ~ 6.0 m (width) by ~ 4.4 m (length) by ~ 2.9 m (height), whereas the spacecraft bus structure is ~ 1 m (width) by ~ 1.6 m (length) by ~ 1.1 m (height).
7. This accuracy is estimated by a combination of the target marker landing dispersion of 40 m for the nominal spacecraft capability, with additional instability due to malfunction of two axes of reaction wheels. For details, see (30).
8. J. Veverka *et al.*, *Nature* **413**, 390 (2001).
9. J. Veverka *et al.*, *Science* **292**, 484 (2001).
10. G. D'Anna *et al.*, *Nature* **424**, 909 (2003).
11. F. Horz, M. Cintala, *Meteor. Planet. Sci.* **32**, 179 (1997).
12. P. Lee, *Icarus* **124**, 181 (1996).
13. P. Michel, M. Yoshikawa, *Icarus* **179**, 291 (2005).
14. A. F. Cheng, N. Izenberg, C. R. Chapman, M. T. Zuber, *Meteor. Planet. Sci.* **37**, 1095 (2002).
15. H. Yano, S. Hasegawa, M. Abe, A. Fujiwara, *Proc. Asteroids, Comets, Meteors 2002 ESA-SP500*, 103 (2003).
16. The 1-m sampler horn comprises an Al metal cylindrical horn of 15-cm diameter at the tip, a deformable cylindrical union, and an Al metal conical horn directed to the sample chamber, all connected by

double-helical springs. The sampling mechanism inside the spacecraft consists of a sample catcher canister, a transfer mechanism to the reentry capsule, and three projectile launchers.

17. In the final sequence of the touchdown, the Hayabusa spacecraft would have (i) synchronized inertial velocity with the asteroid surface by canceling two-dimensional, horizontal velocities with respect to the target marker landing point, (ii) aligned to the local surface slope measured by four LRF-51 beams, (iii) detected the contact with the surface by the tip of the sampler horn attached on the anti-Sun face at ~ 10 cm/s of free-fall vertical velocity, (iv) fired a pair of 5-g Ta projectiles at ~ 300 m/s, (v) fractured surface materials, (vi) collected ejected rock fragments and/or regolith particles, which are concentrated through the conical horn toward the sample canister inside the spacecraft, and (vii) ascended again within a few seconds.
18. A record of the pyrotechnics control device for the projectors did not indicate the completion of firing. However, this report may be faulty as a result of the system power reset that occurred soon after the TD2 ascent due to a temporal attitude control loss by reaction control systems (RCS) fuel leakage.
19. The stiffness of the sampler horn is governed by the double-helical springs, and its laboratory data was obtained by NIPPI Corporation before spacecraft integration.
20. K. Yoshida, T. Kubota, S. Sawai, A. Fujiwara, M. Uo, *Adv. Astronautical Sci.* **108**, Part 1, 481-490, AAS 01-135, (2001).
21. H. Hertz, in *Miscellaneous Papers by H. Hertz*, Jones and Schott, Eds., (London, UK, 1896).
22. G. Gilardi, I. Sharf, *Mechanism Machine Theory* **37**, 1213 (2002).
23. The contact force F_n generated in the surface normal direction is computed by $F_n = k\delta^n$, where k is the stiffness of the surface assumed as a flat plate, δ is a penetration depth of the end tip of the sampler horn into the surface, and $n = 1.5$ is a constant. The friction force was estimated by Coulomb's model as $F_t = \mu F_n$, where F_t is the friction force generated in the surface tangent direction and μ is the kinetic friction coefficient.
24. J. E. Colwell, *Icarus* **164**, 188 (2003).
25. This does not mean that the relative horizontal velocity of the spacecraft (V_x) to the surface is constant for the whole period after the target marker tracking. If that were the case, the spacecraft could have traversed the whole Muses Sea area during the final descent, but that was not what actually occurred. Instead, this result tells us that the residual horizontal velocity was accumulated during the attitude-control maneuvers by the RCS in the final descent, including obstacle avoidance.
26. T. Matsuda, thesis, Tokyo Institute of Technology, Japan (2001).
27. T. Okada *et al.*, *Adv. in Geoscience* **3**, 119 (2006).
28. T. G. Müller, T. Sekiguchi, M. Kaasalainen, M. Abe, S. Hasegawa, *Astro. Astrophys.* **443**, 347 (2005).
29. I. Kushiro, A. Fujiwara, H. Yano (Eds.), *The First Competition for the MUSES-C Asteroidal Sample Preliminary Examination Team, ISAS-SP-16*, ISAS, Japan (2003).
30. T. Kubota *et al.*, *Proc. of 11th Astrodynamics Symp.*, ISAS, Japan, 294, (2001).
31. We thank M. Uo and T. Okudaira of NEC TOSHIBA Space System, H. Morita and K. Shirakawa of NEC Aerospace Systems, S. Yajima of Sumitomo Heavy Industries, T. Takami of Mitsubishi Heavy Industries, and K. Higuchi of JAXA/ISAS for providing the engineering data for the touchdown sequences. We also thank K. Teramoto of the University of Tokyo and C. Honda of JAXA/ISAS for assisting in impact sampling experiments at JAXA/ISAS, and G. Gilardi of Tohoku University for performing simulation analysis of the sampler dynamics. This work is partly supported by the Japan Space Forum Ground-Based Research Grant.

13 February 2006; accepted 10 May 2006
10.1126/science.1126164